ISBN: 978-3-95450-231-8 ISSN: 2673-5490 doi: 10.18429/JACoW-IPAC2023-WEPA018

SYSTEMATIC STUDY OF LONGITUDINAL EXCITATIONS TO INFLUENCE THE MICROBUNCHING INSTABILITY AT KARA

A. Santamaria Garcia *, E. Blomley. E. Bründermann, M. Caselle, P. Schreiber,
L. Scomparin, J. L. Steinmann, A.-S. Müller
Karlsruhe Institute of Technology (KIT), Karlsruhe, Germany

Abstract

Radio-frequency (RF) modulations can influence the microbunching instability (MBI) dynamics and serve to eventually control them with reinforcement learning (RL) methods. Implementing such a feedback system at the Karlsruhe Research Accelerator (KARA) will require that the action decided by the RL agent, in this case an RF modulation, is applied effectively to the electron beam. Such a modulation can be carried out at KARA by two different devices: the kicker cavity of the bunch-by-bunch (BBB) feedback system and the accelerating cavities of the main RF system. The Low-Level RF (LLRF) feedback system would require hardware and firmware modifications to accept the continuous action signal given by the RL agent, so systematic measurements were performed to decide which system should be used in the future. Modulations around different harmonics of the synchrotron frequency were applied and the coherent synchrotron light emitted due to the microbunching dynamics analyzed.

INTRODUCTION

Coherent synchrotron radiation (CSR) occurs when the length of the emitting structure is smaller than the wavelength of the emitted radiation, increasing the spatial coherence between the emitted waves. The intensity of the CSR scales quadratically with the number of electrons in the bunch for ultra-relativistic electrons, giving place to a strongly increased radiation in the THz regime. Intense THz radiation from Gaussian bunches requires root-mean-square (RMS) bunch lengths of 1 ps or below, or the presence of substructures in bunches longer than 1 ps [1]. The zero-current (RMS) bunch length can be reduced in KARA from 21.6 ps to ~2 ps with low momentum compaction α_c optics [2], a regime in which the MBI develops above a certain current threshold I_{thres}. The MBI is a longitudinal collective instability driven by the self-interaction of the bunch with its own CSR wakefield, and results in the formation of substructures which emit bursts of coherent THz radiation [3]. While the increased radiation is desired, the MBI deteriorates the beam properties and limits the bunch current range for stable operation with short electron bunches [4]. The idea of controlling the MBI with RF modulations was explored in [5], where the influence of RF modulations on the CSR emission at KARA was verified in simulation and tested experimentally [6]. In this study, we evaluate the extent of the influence of RF modulations performed with the BBB feedback system on the CSR signal, compared to the LLRF system at KARA. To achieve this, we considered different phase and voltage sinusoidal modulations at frequencies sweeping around the second and third harmonics of the synchrotron frequency.

LONGITUDINAL MODULATION MEASUREMENTS

The measurements were taken in low-α_c optics, with the main parameters summarized in Table 1. The bursting threshold was estimated at $I_{\text{thres}} = [0.15 - 0.18]$ mA, using the standard deviation of the THz signal for the non-modulated cases, as reported in [7, 8] and shown in Fig. 1.

Table 1: Relevant Parameters During the Measurements

Energy	E [GeV]	1.3
Total RF voltage	V_{RF} [kV]	854.3
RF frequency	f_{RF} [MHz]	499.7
Revolution frequency	f_{rev} [MHz]	2.716
Synchrotron frequency	f_{sync} [kHz]	6.9
Momentum comp. factor	α_c	8.3×10^{-3}
Filling pattern	-	single bunch
Current range	I_{bunch} [mA]	0.02 - 0.83
MBI threshold (measured)	I_{thres} [mA]	0.15 - 0.18

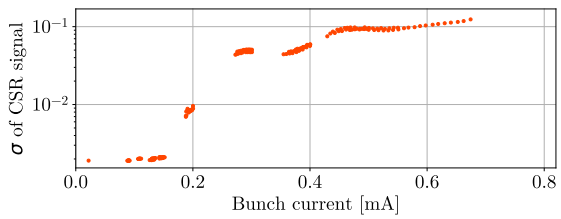

Figure 1: Experimental determination of the onset of the MBI found between 0.15 mA and 0.18 mA.

RF Modulations

To better understand the influence of each modulation on the MBI we can split the total longitudinal potential in three contributions $V_{\text{TOT}} = V_{\text{RF}} + V_{\text{BBB}} + V_{\text{CSR}}$, where the interplay between V_{RF} or V_{BBB} with the distortion driven by V_{CSR} will dictate the longitudinal beam dynamics. The applied voltage V_{mod} and phase ϕ_{mod} modulations are sinusoidal $A_{\text{mod}} \sin(2\pi f_{\text{mod}} t)$ and modify the voltage contributions in the following way

$$V(t) = (V_{\text{mod}} + V_0) \sin(2\pi f_{\text{RF}} t + \phi_{\text{mod}} + \phi_0), \quad (1)$$

where $V(t)$ can be either V_{RF} or V_{BBB}.

* andrea.santamaria@kit.edu

ISBN: 978-3-95450-231-8 ISSN: 2673-5490 doi: 10.18429/JACoW-IPAC2023-WEPA018

The KARA RF system consists of two stations located at diametrically opposite sides of the ring, each station with a klystron driving two cavities. The phase and voltage modulations were carried out using only one of the stations. The BBB feedback system acts in the longitudinal plane through an RF cavity, and the modulations applied were voltage modulations. During these voltage modulations, three different constant BBB backend phases were considered. The original BBB phase (in arb. u.) of 1300 was kept, and two other phases at 150 and 850 were chosen from a phase scan, shown in Fig. 2. The phase scan was performed during a voltage modulation at $f_{\mathrm{mod}} = 2 \cdot f_{\mathrm{sync}}$, and the maximum amplitude seen on the BPM spectrum was recorded and plotted against the phase. We chose two additional phases where the achieved amplitude would be lower or slightly higher than the normal operation phase.

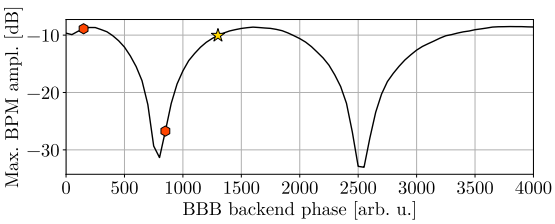

Figure 2: Influence of the BBB phase on the beam during a voltage modulation. The star-shaped marker shows the normal operation phase, and the red markers the two additional phases considered.

A summary of the different RF modulations applied in this study can be found in Table 2. The modulation frequency f_{mod} was varied around the second and third harmonics of the synchrotron frequency f_{sync}. The modulation frequency was changed at steps of 70 Hz within the interval shown in Table 2 to avoid beam splitting for modulations at the exact harmonic [9].

Table 2: Different types of modulations considered during the measurements. Voltage and phase modulations were performed independently.

Mod. type	A_{mod}	$f_{\mathrm{mod}}/f_{\mathrm{sync}}$
BBB V_{mod}	0.69 kV	(2 or 3)±0.2
LLRF V_{mod}	(15, 30, or 45) kV	(2 or 3)±0.2
LLRF ϕ_{mod}	1°, 2°, or 2.5°	(2 or 3)±0.2

Measurement of the CSR Signal

The THz radiation was measured with a broadband Schottky diode, which is an ultra-fast detector with a spectral range of 50 GHz to 1200 GHz and rise time below 100 ps. The pulse detected by the Schottky diode was then digitized with one ADC channel of the KAPTURE-2 board, a data acquisition system for continuous sampling of ultra-short pulses developed at KIT [10]. The high-throughput digitized signal of 12-bit resolution from KAPTURE is handled by HighFlex 2, a custom modular readout card (Xilinx ZYNQ family) that tags the data with the bunch number and sends it through Gigabit Ethernet to the KINGFISHER platform, developed specifically for low-latency feedback with RL methods [11]. An example of the flexibility of the whole data acquisition chain in feedback applications can be found in Ref. [12]. For the measurements presented in this paper, the feature extraction module of KINGFISHER was used to record the relevant accelerator parameters, and each measurement consisted of 2.7×10^6 consecutive recorded turns (1 s of data).

Results at low-α_c

The frequency spectrum was extracted from the measured CSR time signal by applying a fast Fourier transform (FFT) to study the influence of the modulations on the characteristic frequencies of the MBI. These are the *low bursting frequency* and the sometimes called *finger frequency* [13]. The low bursting frequency is the rate of growing and damping of the charge substructures, a periodic phenomenon driven by the equilibrium between the driving wake potential and radiation damping, diffusion, and filamentation mechanisms. This is observed as a periodic fluctuation of the CSR amplitude in time, and a growing and shrinking effect in longitudinal phase space. In this study the low bursting naturally appears at around 500 Hz. The finger frequency is dominant at currents just above the current threshold, disappearing at higher currents, and is related to the number of substructures and their rotation in phase space. In this study the finger frequency appears between 30 kHz and 80 kHz. The main aspect of the instability that we would like to control in the future is the low bursting frequency, which makes the CSR power considerably fluctuate on timescales that are difficult for users to average. To assess the overall influence of the modulations mentioned in Table 2 on the low burst, we looked at the probability distribution of the area of the FFT around this particular frequency interval and at its repetition rate under different modulations, shown in Fig. 3. Concerning the statistics of the FFT area shown at the top of Fig. 3, we can observe that the BBB modulations manage to very slightly increase the area on average compared to the non-modulated case, and that the data distribution is very similar to the non-modulated case. The LLRF modulations show different data distributions, and have the ability to both increase and decrease the area, indicating a larger influence over the emitted power. The difference between modulations becomes more apparent when looking at the rate at which the burst happens, shown in the lower plot of Fig. 3. We see that LLRF modulations can considerably lower the rate at which the bursting occurs, particularly for $A_{\mathrm{mod}} = 30$ kV. From these data we can also conclude that the BBB phase had no relevant influence on the emission. To visualize the effect of the LLRF modulations on the frequency spectrum across different current values, we show a sequence of measurements in Fig. 4. The low burst frequency is dominant as expected, and its center frequency and bandwidth can be seen mainly between 100 Hz and 1 kHz. We observe that LLRF voltage and phase modulations can considerably lower the center frequency of the low burst when the modulation is

ISBN: 978-3-95450-231-8 ISSN: 2673-5490 doi: 10.18429/JACoW-IPAC2023-WEPA018

very near the second harmonic of the synchrotron frequency, and that voltage modulations seem to have a stronger effect than phase modulations. When the modulation frequency is near three times the synchrotron frequency, shown in the central stripe of the plot, we cannot observe any difference in the spectrum.

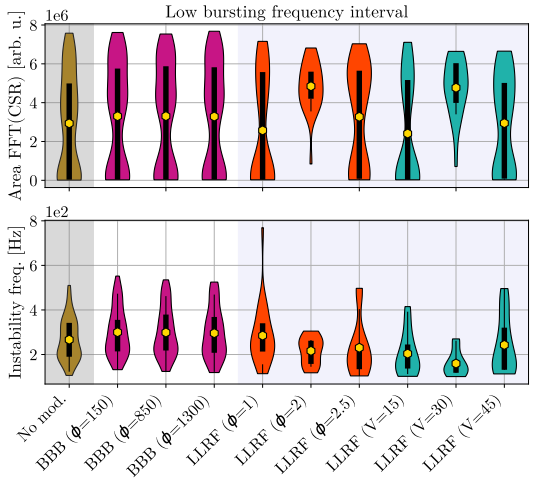

Figure 3: Data distribution of the area of the FFT of the CSR signal in the low bursting frequency interval (top) and the central frequency of the low burst (bottom). The data in the top plot has been normalized to the current of each measurement. All measurements were included in the top plot, and the third harmonic modulations were excluded from the bottom plot. The yellow marker indicates the mean of the distribution, the black box marker the interquartile range, the whiskers the 95% confidence interval, and the vertical shape indicates the probability density.

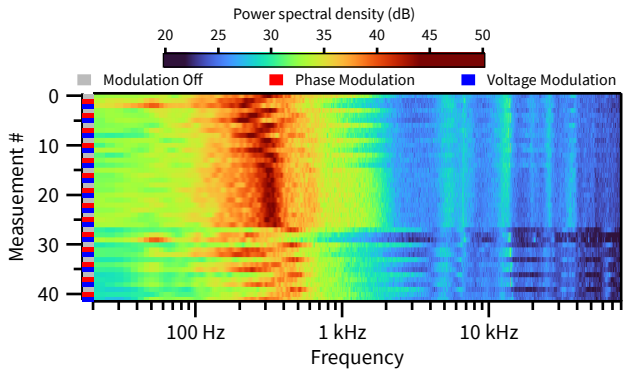

Figure 4: Spectrogram of 41 measurements shown in a vertical sequence, with staggered non-modulated cases (gray marker), LLRF voltage (blue marker), and phase (red marker) modulations at 30 kV and 2°, respectively. The modulations were carried out around $2 \cdot f_{\mathrm{sync}}$, except from #15 to #26 where $f_{\mathrm{mod}} \sim 3 \cdot f_{\mathrm{sync}}$. The current across measurements decayed from 0.5 mA to 0.4 mA.

Finally, we look at the time signals and corresponding FFTs of a particular set of measurements to better understand in which other ways the modulations might be influencing the CSR emission, shown in Fig. 5. We can observe that the LLRF phase modulation has a major influence on the CSR emission, damping the low burst and reducing its rate, as well as diffusing the substructures related to the finger frequency, visible at 35 kHz and 65 kHz for the no modulation and BBB cases. The LLRF voltage modulation has a similar effect to the phase modulation, with the difference that it manages to excite the higher order harmonics of the modulation frequency, visible as peaks. These harmonics could also be an artifact of the acquisition. If the excitation induces a coherent bunch motion in the longitudinal plane, the arrival time of the pulse will jitter and KAPTURE (in single channel mode) will not always sample the peak of the pulse, which would be seen as harmonics of the excitation frequency. We could resolve the pulse peak by using the four channels of KAPTURE, and verify that the harmonics come from the beam dynamics. We cannot observe any discernible change between no modulation and the BBB modulation.

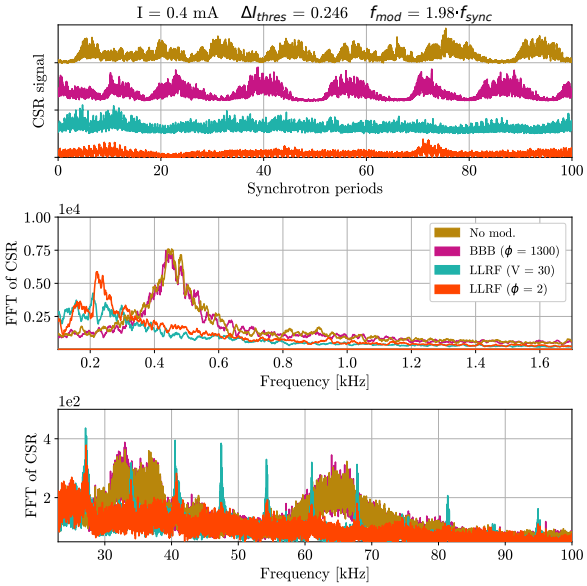

Figure 5: Set of different modulations performed sequentially at 0.4 mA, with $f_{\mathrm{mod}} = 1.98 \cdot f_{\mathrm{sync}}$. Top: time signals of the CSR recorded with KAPTURE, where one synchrotron period is equivalent to 399.7 turns. Middle and bottom: FFT of the CSR signal in the low burst frequency region and in the finger frequency region, respectively. The CSR and FFT values are given in arbitrary units.

OUTLOOK

While the BBB feedback system at KARA has a flexible backend that can process continuous modulation signals and can act on a bunch-by-bunch basis, it does not have the capacity to sufficiently influence the MBI. The LLRF system cannot act on multiple bunches individually, but has yielded very promising results. Its firmware and hardware will be modified in the near future to accept the external modulation signal given by an RL algorithm.

ACKNOWLEDGEMENTS

A. Santamaria Garcia acknowledges funding by the BMBF ErUM-Pro project TiMo (FKZ 05K19VKC).

ISBN: 978-3-95450-231-8 ISSN: 2673-5490 doi: 10.18429/JACoW-IPAC2023-WEPA018

REFERENCES

[1] A.-S. Müller and M. Schwarz, "Accelerator-Based THz Radiation Sources," in *Synchrotron Light Sources and Free- Electron Lasers: Accelerator Physics, Instrumentation and Science Applications*, 2020, pp. 83–117. doi:10.1007/978-3-030-23201-6_6

[2] A. I. Papash *et al.*, "Non-Linear Optics and Low Alpha Operation at the Storage Ring KARA at KIT", in *Proc. IPAC'18*, Vancouver, Canada, Apr.-May 2018, pp. 4235–4238. doi:10.18429/JACoW-IPAC2018-THPMF070

[3] G. Stupakov and S. Heifets, "Beam instability and microbunching due to coherent synchrotron radiation," *Phys. Rev. ST Accel. Beams*, vol. 5, p. 054402, 2002. doi:10.1103/PhysRevSTAB.5.054402

[4] M. Brosi, "Overview of the Micro-Bunching Instability in Electron Storage Rings and Evolving Diagnostics", in *Proc. IPAC'21*, Campinas, Brazil, May 2021, pp. 3686–3691. doi:10.18429/JACoW-IPAC2021-THXA02

[5] T. Boltz, "Micro-Bunching Control at Electron Storage Rings with Reinforcement Learning," Ph.D. dissertation, 2021. doi:10.5445/IR/1000140271

[6] T. Boltz *et al.*, "Excitation of Micro-Bunching in Short Electron Bunches Using RF Amplitude Modulation", in *Proc. IPAC'21*, Campinas, Brazil, May 2021, pp. 3173–3176. doi:10.18429/JACoW-IPAC2021-WEPAB233

[7] P. Schönfeldt *et al.*, "Comparison of Different Approaches to Determine the Bursting Threshold at ANKA", in *Proc. IPAC'13*, Shanghai, China, May 2013, paper MOPEA020, pp. 112–114.

[8] M. Brosi *et al.*, "Fast mapping of terahertz bursting thresholds and characteristics at synchrotron light sources," *Phys. Rev. Accel. Beams*, vol. 19, p. 110701, 2016. doi:10.1103/PhysRevAccelBeams.19.110701

[9] J. L. Steinmann *et al.*, "Increasing the Single-Bunch Instability Threshold by Bunch Splitting Due to RF Phase Modulation", in *Proc. IPAC'21*, Campinas, Brazil, May 2021, pp. 3193–3196. doi:10.18429/JACoW-IPAC2021-WEPAB240

[10] M. Caselle *et al.*, "KAPTURE-2. A picosecond sampling system for individual THz pulses with high repetition rate," *J. Instrum.*, vol. 12, no. 01, p. C01040, 2017. doi:10.1088/1748-0221/12/01/C01040

[11] L. Scomparin *et al.*, "KINGFISHER: A Framework for Fast Machine Learning Inference for Autonomous Accelerator Systems", in *Proc. IBIC'22*, Kraków, Poland, Sep. 2022, pp. 151–155. doi:10.18429/JACoW-IBIC2022-MOP42

[12] L. Scomparin *et al.*, "A low-latency feedback system for the control of horizontal betatron oscillations", presented at the IPAC'23, Venice, Italy, May 2023, paper THPL027, this conference.

[13] M. Brosi, "In-Depth Analysis of the Micro-Bunching Characteristics in Single and Multi-Bunch Operation at KARA," Ph.D. dissertation, Karlsruher Institut für Technologie (KIT), 2020. doi:10.5445/IR/1000120018